Size-dependent Kinetics Determination of MoS_2-K_2O/CNTS Nanocatalyst in the Synthesis of Alcohols from Syngas

Saba Karimi, Rohollah M. Keaei, and Ahmad Tavasoli*

School of Chemistry, College of Science, University of Tehran, Tehran, Iran

ABSTRACT

The influence of Mo particle size on the catalytic activity and product selectivity of alkalized MoS_2 nanocatalysts has been investigated. Nanocatalysts are prepared using a microemulsion technique with water-to-surfactant ratios of 1-12. Three different techniques, including XRD, TEM, and hydrogen chemisorption were used to determine the molybdenum average particle size and their activity and selectivity in higher alcohols synthesis (HAS) carried out in a fixed bed microreactor at 330 °C and 70 bar. To fix the percentage of CO conversion, the GHSV is changed from 3.6 to 2.57 (nl/(hr.g catalyst)). The average MoS_2 particle sizes are changed from 4.5 to 11.9 nm. The experimental results showed that changing particle size from 11.9 to 4.5 nm decreased the methanol formation rate from 0.00634 to 0.00534 (mol/(hr.g catalyst)) but increased ethanol formation rate from 0.00581 to 0.00787 (mol/(hr.g catalyst)) and higher alcohols formation rate from 0.00473 to 0.00657 (mol/(hr.g catalyst)). A size-dependent kinetics model was developed to calculate the alcohol formation rates versus catalyst average particle size. The model not only matched experimental and theoretical results, but also showed that MoS_2 catalyst had size-dependent structure and for the prediction of product selectivity it was easier to use this mathematical model.

Keywords: Higher Alcohol, Rate, Selectivity, Particle Size, Size-dependent Kinetics

INTRODUCTION

Higher alcohols synthesis (HAS) from syngas, an economically attractive method for making fuels and chemicals, is interested due to the enhancement of petroleum price, environmental concerns, and additive for gasoline to increase octane number. Among different methods for higher alcohols synthesis, the molybdenum disulfide (MoS_2) catalyst mainly produces hydrocarbons but, when it is promoted with alkali metals, it can produce alcohols from syngas. The function of alkali metals is to reduce the hydrogenation ability of alkyl species to form alkanes and increase the sites active for the formation of alcohols [1-5].

Some investigations have been carried out to study the influence of catalyst physico-chemical properties on higher alcohols synthesis and gain a better understanding of the structure-sensitive effects in HAS catalysis [6-8]. A sub-category of structure-sensitive reactions regards the dependence of both catalytic activity and selectivity on catalytic metal particle size. Bezemer et al. showed that in Fischer-Tropsch

***Corresponding author**
Ahmad Tavasoli
Email: tavassolia@khayam.ut.ac.ir
Tel: +98 912 298 8426
Fax: :+98 21 6649 5291

Article history
Received: December 15, 2013
Received in revised form: August 9, 2014
Accepted: August 18, 2014
Available online: February 20, 2015

synthesis, activity and selectivity towards C_{5+} are higher in the case of smaller particles. They presented sizes of 6-8 nm as the optimum range for active metal particles size [9].

The thermodynamic analysis of the effect of nanoparticle size on adsorption equilibrium and rates was initiated by Parmon [10]. Studying catalysts surface and trying to improve the properties of surface to have catalysts with better quality include a large area in recent researches. The main focus is placed on the analysis of the nanoparticle size influence on reaction rates and kinetic regularities in order to obtain kinetic expressions, which could primarily be used for engineering purposes [11, 12]. The experimental data of catalytic activity versus the average particle radius for Fischer-Tropsch synthesis by cobalt supported on carbon nanofibers showed good correspondence between the theory and experiments [13].

Tae et al. developed a mechanistic kinetic model to describe the synthesis of mixed alcohol from syngas over 17 wt.% K_2CO_3-promoted MoS_2 catalyst [14]. Also, Surisetty et al. studied the intrinsic kinetics of the higher alcohol synthesis reaction from synthesis gas over an alkalized Co-Rh-Mo catalyst supported on multi-walled carbon nanotubes [15]. However, the size-dependent intrinsic kinetic model of higher alcohol synthesis from synthesis gas based on different particle sizes of the metal particles has never been investigated.

Microemulsion, a novel technique for catalyst preparation, enables the control of metal particle size with a narrow particle size distribution, regardless of metal content [16-19]. Briefly, a microemulsion consists of nanosized water droplets surrounded by an oil phase, stabilized by a surfactant [19]. The size of the metal particles formed in water-in-oil (w/o) microemulsion can be controlled by changing the micelle size (the water-to-surfactant ratio) [19].

In this study, a theoretical analysis addressing the impact of the changes in chemical potential upon adsorption is performed. The quantitative model is illustrated by comparing the experimental data of catalytic activity versus the average particle size. Main products include methanol, ethanol, propanol, and butanol obtained by experiments using MoS_2 catalysts supported on carbon nanotubes (CNT's). Activity analysis on different particle sizes was performed for the case of consecutive mechanism suggested for overall reactions, demonstrating that significant changes could be anticipated in this case. Provided analysis suggested that thermodynamic analysis could be invoked for the explanation of nanokinetics, e.g. structure sensitivity and other kinetic regularities dependence on the size of catalytic nanoclusters.

EXPERIMENTAL

Preparation of Catalysts

Multi-walled CNT's (purity >95%) were used as the support for the preparation of the catalysts. Prior to catalyst preparation, the support was treated with 30% HNO_3 refluxed at 120 °C overnight, washed with distilled water several times, and finally dried at 120 °C for 6 hrs (the characteristics are shown in Table 1). The catalysts were prepared by a microemulsion method. Molybdenum and potassium particles were synthesized in a reverse microemulsion using a nonionic surfactant Triton X-100 and n-hexanol as the oil phase. The concentrations of molybdenum and potassium were adjusted using aqueous solutions of $(NH_4)_6Mo_7O_{24}.4H_2O$ (Merck) and K_2CO_3 at a molybdenum and potassium concentration of 15 and 8 wt.% respectively. The water-to-surfactant (W/S) molar ratios were selected as 1, 4, 8, and 12. After 15-minute vigorous stirring, microemulsions were obtained. Then, hydrazine was added to the solutions to develop nanoparticle formation in the core of the micelles by reducing the metal oxides. Next, the purified carbon nanotubes were added under stirring. Afterwards, tetrahydrofurane

(THF) was added to the solutions dropwise (1 ml/min). The mixtures were left to mature and settle slowly overnight and then decanted. The samples were filtered and washed several times with ethanol. Subsequently, the catalysts were dried at 120 °C, calcined under argon flow at 450 °C for 3 hrs, and slowly exposed to an oxygen atmosphere during the cooling step. The catalysts prepared were signified as Cat1, Cat2, Cat3, and Cat4 (see Table 1).

Analysis Methods

ICP-OES

The metal loadings of the purified support and calcined catalysts were performed using Varian VISTA-MPX inductively coupled plasma-optical emission spectrometry (ICP-OES) instrument.

BET Surface Area Measurements/BJH Pore Size Distributions

Surface area, pore volume, and pore average diameter of the support and calcined catalysts were measured using an ASAP-2010 V_2 Micrometrics system. The samples were degassed at 200 °C for 4 hrs under a 50-m Torr vacuum and their BET area, pore volume, and pore diameter was determined.

Transmission Electron Microscopy (TEM)

The morphology of the purified support and catalysts were studied by transmission electron microscopy (TEM). Sample specimens for TEM studies were prepared by ultrasonic dispersion of the catalysts in ethanol and the suspensions were dropped onto a carbon-coated copper grid. TEM investigations were carried out using a Philips CM_20 (100 kV) transmission electron microscope equipped with a NARON energy-dispersive spectrometer with a germanium detector.

X-ray Diffraction (XRD)

The phases and particle sizes of the crystals present in the catalysts were analyzed by XRD using a Philips Analytical X-ray diffractometer (XPert MPD) with monochromatized Co/Kα radiation, 2θ angles from 20° to 80°. The Debye–Scherer formula ($d = 0.9\lambda/\beta\cos\theta$, where β is full width at half maximum (FWHM), λ is the wave length of X-ray, 0.9 is a constant) was applied to MoS_2 peaks at 2θ = 43.3° (the most intense peak for MoS_2), in order to calculate the average particle sizes.

Hydrogen Chemisorption

For all the catalysts, the amount of chemisorbed hydrogen was measured using Micrometrics TPD-TPR 2900 analyzer system. 0.2 g of the calcined catalyst was first purged in a flow of argon at 140 °C to remove traces of water.

The temperature was then raised to 500 °C at a linearly programmed rate of 10 °C/min and the catalyst was reduced for 12 hrs under hydrogen flow and then cooled to 40 °C. Then, the flow of hydrogen was switched to argon for 30 min in order to remove the weakly adsorbed hydrogen.

Table 1: Textural properties of the purified CNT's and calcined catalysts

Sample	Preparation route	W/S Ratio	BET surface area (m^2/g)	Total pore volume (ml/g)	Average pore diameter (Å)
CNTs	-	-	252.6	0.59	94.12
Cat1	Microemulsion	1	165	0.468	127
Cat2	Microemulsion	4	142	0.437	128
Cat3	Microemulsion	8	136	0.426	129
Cat4	Microemulsion	12	132	0.419	129

Afterwards, the temperature programmed desorption (TPD) of the samples was performed by increasing the temperature of the samples, with a ramp rate of 40 °C/min, to a maximum temperature of 500 °C under the argon flow. The temperature programmed desorption spectrum was used to determine the molybdenum dispersion and its average crystallite size.

Reaction Setup and Experimental Procedure

Higher alcohol synthesis was performed in a tubular down flow, fixed bed microreactor system. The reactor was made up of an Inconel tube with a length and inside diameter of 450 and 22 mm respectively. The reactor temperature was controlled via a PID temperature controller. Brooks 5850 mass flow controllers were used to add H_2 and CO at the desired rate to the reactor. The reactor was packed with 0.5 g of the catalyst diluted with silicon carbide having a mesh size of 90 and housed in a molten salt bath controlled by a temperature controller. The reactor was pressurized to 30 bar with He and the reduction, as well as the sulfurization, was carried out for 6 hrs at 450 °C at a heating rate of 2 °C/min using a gas mixture containing 5 mol.% H_2S in H_2 and a flow rate of 50 ml/min. The temperature was then lowered to the reaction temperature, and the system was pressurized to the reaction condition. The feed gas mixture (H_2/CO ratio of 2) was passed through mass flow controllers and the HAS reaction was carried out in a steady state under the reaction conditions of 320 °C and 70 bar over a period of 48 hrs. In the case of Cat1 catalyst, the gas hourly space velocity is adjusted at 3.6 nl/(hr.gr catalyst). However, in order to have a constant percentage of feed conversion for all the experiments, the gas hourly space velocity is decreased to 3, 2.7, and 2.57 nl/(hr.gr catalyst) for Cat2, Cat3, and Cat4 catalysts respectively. The product gas was cooled to 0 °C and separated into gas and liquid phases at the reaction pressure. The CO, CO_2, and other gaseous products were monitored with time intervals of 1 hr. The products were collected after the completion of the run and analyzed by means of three gas chromatographs, a Shimadzu 4C gas chromatograph equipped with two subsequent connected packed columns: Porapak Q and Molecular Sieve 5Å, and a thermal conductivity detector (TCD) with argon which was used as a carrier gas for hydrogen analysis. A Varian CP 3800 with a chromosorb column and a thermal conductivity detector (TCD) were used for CO, CO_2, CH_4, and other non-condensable gases. A Varian CP 3800 with a Petrocol Tm DH100 fused silica capillary column and a flame ionization detector (FID) were used for liquid products so that a complete product distribution could be provided.

Size-dependent Kinetic Model

Alcohol synthesis from syngas over alkalized MoS_2 nanoparticles is initiated and developed by the adsorption of reactants over active sites. The following mechanism describes HAS over this catalyst [14]:

Initiation:

$$CO + s \longleftrightarrow COs \qquad K_1, k_1, k_{-1} \qquad (1)$$

$$H_2 + 2s \longleftrightarrow 2Hs \qquad K_2, k_2, k_{-2} \qquad (2)$$

$$COs + Hs \longleftrightarrow CHOs + s \qquad K_3, k_3, k_{-3} \qquad (3)$$

$$CHOs + Hs \longleftrightarrow CH_2Os + s \qquad K_4,\ k_4,\ k_{-4} \qquad (4)$$

$$CH_2Os + Hs \longleftrightarrow R_1Os + s \qquad K_5,\ k_5,\ k_{-5} \qquad (5)$$

Chain growth

$$R_iOs + COs \longrightarrow R_iCOO + s \quad k_6, \quad i = 1, \ldots, 4 \qquad (6)$$

$$R_iOs + 2Hs \longrightarrow R_is + H_2O + 2s \quad k_7, \quad i = 1, 2, \ldots, 8 \qquad (7)$$

$$R_is + COs \longrightarrow R_iCOs + s \quad k_8, \quad i = 1, 2, \ldots 5 \qquad (8)$$

$$R_iCOs + 2Hs \longrightarrow R_i + 1Os + 2s \quad (9)$$
$$k_9 \quad i = 1,2,\ldots,4$$

Termination

$$R_iOs + Hs \longleftrightarrow R_iOH + 2s \quad (10)$$
$$k_{10},\ k_{-10} \quad i = 1,2,...,4$$

$$R_iCOOs + Hs \longrightarrow R_1COOR_i - 1 + 2s \quad (11)$$
$$k_{11} \quad i = 1,2,\ldots,4$$

$$R_is + Hs \longrightarrow C_iH_{2i} + 2s \quad (12)$$
$$k_{12} \quad i = 1,2\ ,...,8$$

$$R_is \longrightarrow C_iH_{2i} + Hs \quad (13)$$
$$k_{13} \quad i = 1,2,...,5$$

Based on the above mechanism, Park et al. derived a kinetic model for mixed alcohol synthesis from syngas over unsupported K/MoS_2 catalyst [14]. Based on the model derived by Park, the rate equations for the formation of alcohols (ri^{OH})), paraffins (ri^{P}), olefins (ri^{O}), esters (ri^{E}) can be written as:

$$ri^{OH} = \frac{\lambda_2 P_{H_2}^{0.5}\theta_{R_iO}}{Ads} - \frac{\lambda_5 P_i(OH)}{Ads^2} \quad (14)$$

Since the produced alcohols can be consumed in the next reactions, the rate expression for alcohol synthesis using this model has two terms. In this model P_{H_2} is hydrogen partial pressure, λ_2 and λ_5 are the kinetic parameter groups defined by equilibrium and rate constants and relate to the production and consumption of alcohols respectively; P_i(OH) is alcohol average partial pressure and *Ads* denotes the adsorption term as:

$$Ads = 1 + K_1P_{CO} + \left(K_2P_{H_2}\right)^{0.5} + K_1K_2^{0.5}K_3P_{CO}P_{H_2}^{0.5} + K_1K_2K_3K_4P_{CO}P_{H_2} + \lambda_4P_{CO}P_{H_2}^{3/2} \quad (15)$$

θ_{Rio} is surface coverage for surface species of R_iO and *i* (*i*= 1-4) is the number of carbon in alcohol.

$$\theta_{R_iO} = \frac{\lambda_4 P_{CO} P_{H_2}^{\frac{3}{2}}}{Ads} \quad (16)$$

$$\theta_{R_iO} = \frac{\left[(\frac{\lambda_8}{\lambda_9})\theta_{R_{(i-1)}CO}P_{H_2} + \lambda_5 P_i^{OH}\right]}{\left[(\lambda_1P_{CO} + \lambda_2P_{H_2}^{\frac{1}{2}})Ads + \lambda_3P\right]} \quad (17)$$

i=2, 3, 4

$$\theta_{RiCO} = \frac{\lambda_5 P_{CO} Ads\theta_{R1}}{P_{H2}} \quad i=2,3,4 \quad (18)$$

$$\theta_{(R_i)} = \frac{(\lambda_3\theta_{RiO}P_{H2})}{(\lambda_7P_{H_2}^{0.5} + \lambda_8P_{CO} + k_{13}Ads)Ads} \quad (19)$$

i=1, 2, 3, 4

where,

$$[s]_0 = [s] + K_1P_{CO}[s] + (K_2P_{H_2})^{\frac{1}{2}}[s] + K_1K_2^{\frac{1}{2}}K_3P_{CO}P_{H_2}^{\frac{1}{2}}[s] + K_1K_2K_3K_4P_{CO}P_{H_2}[s] + \lambda_4P_{CO}P_{H_2}^{\frac{3}{2}}[s] \quad (20)$$

$$[s] = \frac{[s]_0}{Ads} \quad (21)$$

$$K_A = K_3K_1K_2^{\frac{1}{2}} \quad MPa^{-1.5} \quad (22)$$

$$K_B = K_4K_3K_2K_1 \quad MPa^{-2} \quad (23)$$

Using the above equations, the size-independent alcohol formation rates for methanol, ethanol, propanol, and butanol are obtained by:

$$r_{CH_3OH} = \left[\frac{\lambda_2P_{H_2O}^{\frac{1}{2}}\theta_{R_iO}}{Ads}\right] - \left[\frac{\lambda_5P_{CH_3OH}^{\frac{1}{2}}}{Ads^2}\right] \quad (24)$$

In our previous work, we used the kinetic model derived by Park, for the MoS_2-K_2O/CNT's catalyst supported on carbon nanotubes. The calculated kinetic parameters are shown in Table 2 [20]. These parameters are size-independent.

During adsorption reaction (hydrogen is adsorbed in a dissociated form with a stoichiometry of one H per surface Mo atom (stoichiometric factor equal to 0.5)) on catalysts particle, the chemical potential of surface, which expresses the

incremental energy content of a system per unit particulate mass, changes.

Table 2: Calculated kinetic parameters for MoS_2-K_2O/CNT's catalyst [20]

Parameter	Value	Unit
K_1	4.261	MPa^{-1}
K_2	1.049	MPa^{-1}
K_A	0.042	$MPa^{-1.5}$
K_B	0.072	MPa^{-2}
λ_1	0.070	Mol. kg $cat^{-1}.h^{-1}.MPa^{-1}$
λ_2	18.56	Mol.kg-$cat^{-1}.h^{-1}.MPa^{-0.5}$
λ_3	3.210	Mol.kg-$cat^{-1}.h^{-1}.MPa^{-1}$
λ_4	0.0712	$MPa^{-2.5}$
λ_5	91.56	Mol.kg-$cat^{-1}.h^{-1}.MPa^{-1}$
λ_6	0.321	$MPa^{-0.5}$
λ_7	11.21	Mol.kg-$cat^{-1}.h^{-1}.MPa^{-0.5}$
λ_8	7.860	Mol.kg-$cat^{-1}.h^{-1}.MPa^{-1}$
λ_9	0.041	dimensionless
k_{13}	0.158	Mol.kg-$cat^{-1}.h^{-1}$

Thus it can be assumed that, for a cluster comprising more than 100 atoms, the properties determined by the chemical potential can be described somewhat sufficiently using continuous phase thermodynamics. The chemical potential μ_i(r) of a substance *i*, which is also dependent on the radius *r*, can be expressed by [10]:

$$\mu_i(r) = \mu_\infty + \frac{2\sigma V_M}{r} = \mu_\infty + \delta(r) \quad (25)$$

where, V_m is the partial molar volume of the substance forming the condensed phase; σ, μ_∞, and δ represent surface tension, the standard chemical potential of the bulk phase, and chemical potential increment respectively. Upon adsorption on nanoclusters, changes in the Gibbs free energy should also account for the chemical potential changes [12]:

$$\Delta G_{ads}(r) = \Delta G_{(ads)\infty} + \mu_i(r) - \mu_\infty \quad (26)$$

According to reaction mechanism, adsorption and desorption are elementary reactions in higher alcohol synthesis. Linear free energy (Brønsted-Evans-Polanyi) relationship is widely used in homogeneous and heterogeneous catalyzed reactions in the form which relates reaction constants *k* with equilibrium constants *K* in a series of analogous elementary reactions:

$$k = gK^\alpha \quad 0 < \alpha < 1 \quad (27)$$

where, *g* and α are Polanyi parameters and they are constant for a series of reactions and for MoS_2-K_2O/CNT's catalyst α is equal to 0.5 [12]. Equilibrium constant and Gibbs free energy are related by:

$$K(r) = \exp\left(\frac{-\Delta G(r)}{RT}\right) \quad (28)$$

Replacing Gibbs free energy from Equation 28 in Brønsted Equation 27 gives:

$$K(r) = g\exp(-\Delta G_\infty)\exp\left(\frac{-\alpha\delta_{(r)}}{RT}\right) = k\exp\left(\frac{-\alpha\frac{(2\sigma V_m)}{r}}{RT}\right) = k\exp\left(\frac{-\alpha\eta}{r}\right) \quad (29)$$

where,

$$\eta = \frac{2\sigma V_m}{RT} \quad (30)$$

In Equation 42, $k(r)$ indicates size-dependent kinetic constant and *k* is named size-independent kinetic constant. e-$\alpha\eta/r$ is the size-dependent part of kinetic constant. The surface tension of metals is within a range of 1-2 J/m^2 [12]. The molar volume of catalytically active metals is within a range of 6-10 cm^3/mol. Therefore, the value of parameter η for MoS_2-K_2O/CNT's catalyst is 15.32 nm.

Based on the above discussion, in higher alcohol synthesis mechanism shown (Equations 1-13), each step has size-independent rate constant or size-independent equilibrium constant. Multiplying mentioned size-independent rate constants by *e*-

$\alpha\eta/r$ creates new rate constants which is dependent on particle size. For example, for the first step (reversible adsorption of CO over catalyst), consider $K_1(r)$ as size-dependent equilibrium constant. The forward reaction is adsorption and size-dependent rate constant is defined as:

$$k_1(r) = k_1 e^{\frac{-\alpha\eta}{r}} \quad (31)$$

The reverse reaction is desorption and its size-dependent rate constant is defined as:

$$k_{-1}(r) = k_{-1} e^{\frac{(1-\alpha)\eta}{r}} \quad (32)$$

For this reaction, using Equation 31 and 32 gives the size-dependent equilibrium constant as follows:

$$K_1(r) = K e^{\frac{-\eta}{r}} \quad (33)$$

Equations similar to Equations 31-32 can be written for the other steps of the reaction. Substituting independent rate constants with the size-dependent rate constants used in the above equations give the size-dependent alcohol formation rates for methanol, ethanol, propanol, and butanol.

RESULTS AND DISCUSSION

Experimental Results and Model Implementation

The textural properties of the purified carbon nanotubes as well as the results of surface area measurements for the calcined catalysts are given in the Table 1. These results show that the BET surface areas of the Cat1-Cat4 catalysts are 165, 142, 136, and 132 m^2/g respectively. Moreover, the results indicate some more pore blockage by metal oxide clusters in the catalysts prepared at higher water/surfactant ratios.

The elemental compositions of the calcined catalysts measured by ICP are given in Table 3. The measured contents of the prepared catalysts are found to be slightly lower compared to the targeted values. The discrepancies may be due to the dilution of Mo, because of the hygroscopic nature of the Mo precursor.

Table 3: Chemical Composition of the Calcined Catalysts

Catalyst	Targeted Composition (wt. %)		Measured Composition (wt. %)	
	Mo	*K*	Mo K	*K*
Cat1	15	8	14.18	7.78
Cat2	15	8	14.28	7.85
Cat3	15	8	14.28	7.84
Cat4	15	8	14.30	7.90

Three techniques, including TEM, XRD, and hydrogen chemisorption were used to determine the molybdenum average particle size. Figure 1 presents the TEM image of the purified support. As shown, the treated support is comprised of an interwoven matrix of multi-walled CNT's. The TEM images of the Cat1-Cat4 catalysts are shown in Figure 2. As can be seen, very small particles are dispersed mostly inside the tubes and on the outer surface of the CNT's walls. The particle size distribution is also narrow. Indeed, the narrow inner diameter of the CNT channels (8–12 nm) restricted the insertion of particles in sizes close to the channel diameter (10 nm). Particles located outside the nanotubes have grown more. The sizes of particles are within the range of 2-7, 3-9, 5-16, and 5-23 nm for the Cat1, Cat2, Cat3, and Cat4 catalysts respectively.

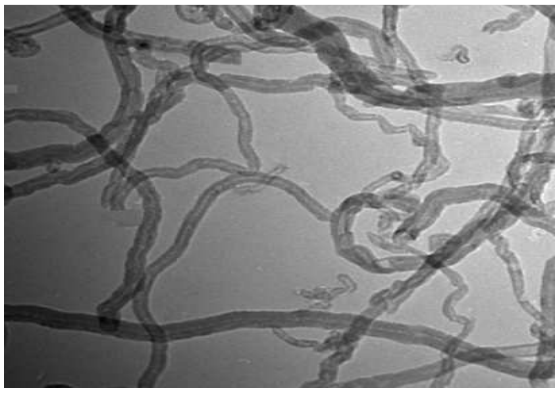

Figure 1: TEM image of the purified CNT's

Figure 3 depicts the size distribution of the particles for Cat1-Cat4 catalysts, which is determined using the population of the total particles of the catalyst based on data taken from 5 TEM pictures. According to this figure, the average particle size for the Cat1, Cat2, Cat3, and Cat4 catalysts are 4.6, 5.5, 9.1, and 11.6 nm respectively.

To determine the crystalline phases, the X-ray diffraction experiments (XRD) of the calcined catalysts were performed. Figure 4 presents the XRD spectrum of the catalysts with different preparation methods. As shown in this figure, in the case of the catalyst prepared by maximum water to surfactant ratio, i.e. Cat4, the intensity of the peaks corresponding to MoO_3 (peaks at 2θ values of 43.3°, 63.2°, and 71.9°) is higher than that of the other catalysts, indicating the greater cluster sizes of MoS_2.

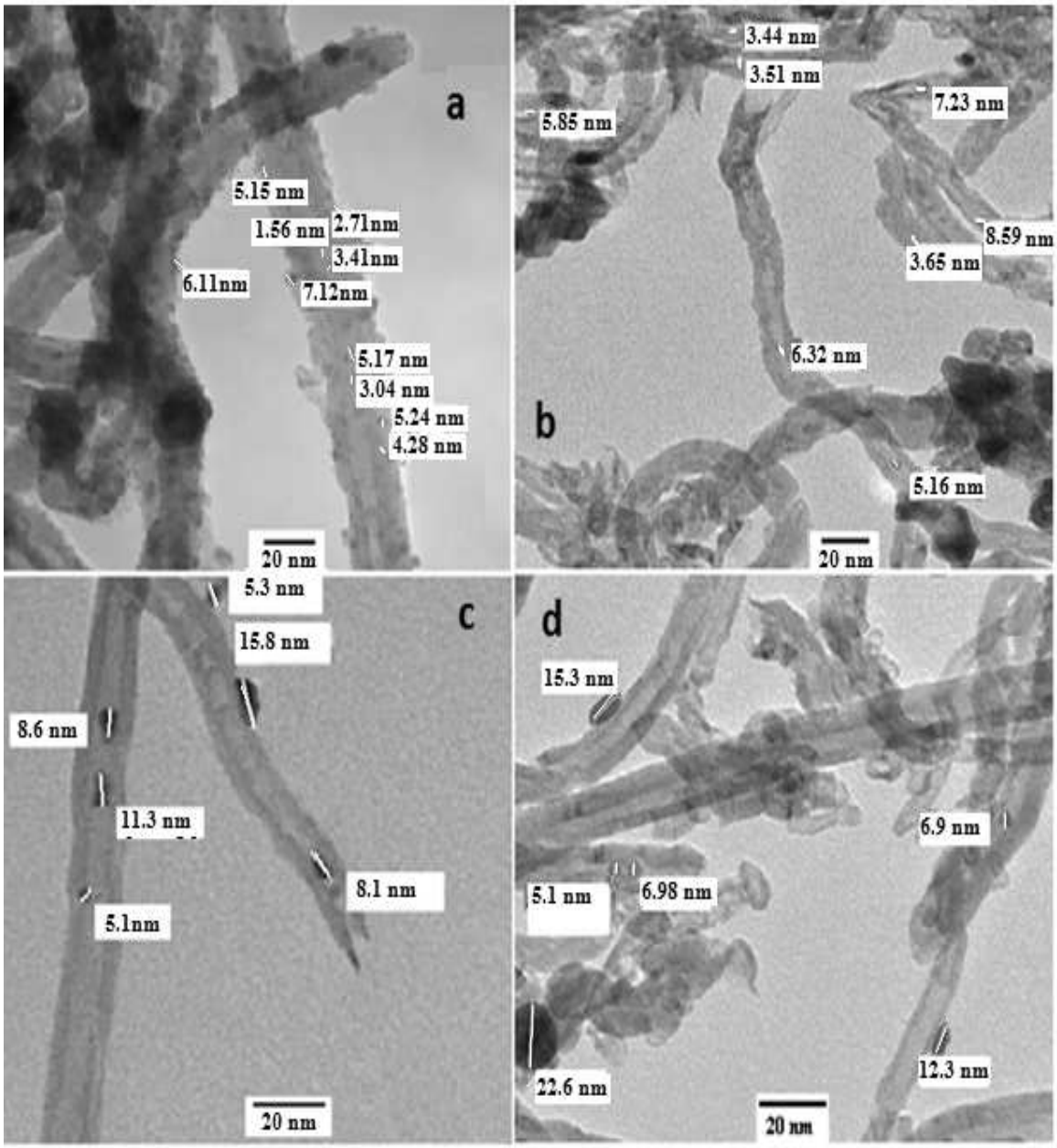

Figure 2: TEM image of the a) TEM image of Cat1 (W/S =1); b) TEM image of Cat2 (W/S =4); c) TEM image of Cat3 (W/S =8); d) TEM image of Cat4 (W/S =12).

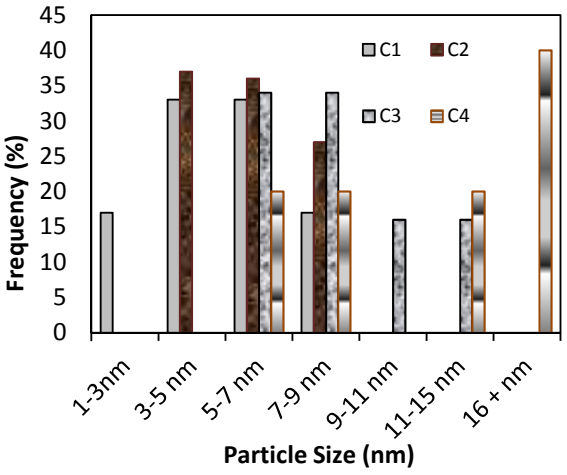

Figure 3: Particles size distribution for Cat1-Cat4 catalysts

This figure also shows that decreasing water to surfactant ratio decreases the intensity of the peaks corresponding to MoO_3, which represents a drop in MoS_2 cluster sizes at smaller W/S ratios. Table 4 shows the average sizes of MoO_3 crystals calculated from the XRD patterns, using the Debye–Scherer formula at a 2θ value of 43.3°. The data agrees reasonably well with the particle diameter obtained with the TEM results. As can be seen, the catalyst prepared at the maximum W/S ratio (a W/S ratio of 12) has the largest crystal sizes, while the catalyst prepared at the minimum W/S ratio (a W/S ratio of 1) has the smallest particle sizes. In accordance with the TEM results, these data confirm that using a microemulsion technique at low W/S ratios decreases the average crystal diameter of MoO_3 significantly. The average particle sizes are linearly correlated with the W/S ratio used during the microemulsion catalyst preparation process. In fact, nanoparticles are formed in the internal structure of the microemulsion, which is determined by the ratio of W/S. At high oil concentration, the bicontinuous phase is trans-formed into a structure of small water droplets within a continuous oil phase (reverse micelles), when surfactant is added. Thus the results show that the size of different droplets determines the MoS_2 particle size, depending on the amount of surfactant [19].

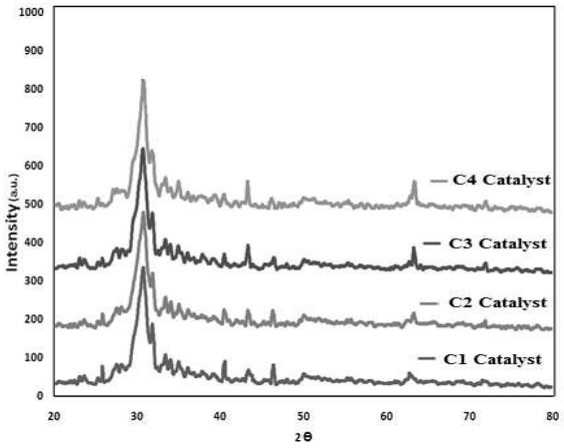

Figure 4: XRD patterns of the calcined catalysts (Cat1-Cat4)

Table 4: Particle sizes of the calcined catalysts

Catalyst	*dp* (nm) calculated by Debye–Scherer formula
Cat1	4.7
Cat2	6.0
Cat3	9.8
Cat4	12.2

The results of hydrogen chemisorption tests are given in Table 5. As shown, lowering W/S ratio considerably increased the hydrogen uptake and the percentage of dispersion. Maximum dispersion is achieved at the minimum W/S ratio of 1. The particle diameter decreases, which is in agreement with the results of XRD and TEM tests. The data agrees reasonably well with the particle diameter obtained with the TEM and XRD results. Higher dispersions and smaller molybdenum cluster sizes in the case of the catalysts prepared at low W/S ratio will increase the number of sites available for CO conversion and raises alcohols formation reaction rates.

Table 5: H_2 chemisorption results for the calcined catalysts

Catalyst	μ mole H_2 desorbed/ g. cat	Dispersion (%)	dP (nm)
Cat1	534	60.75	4.5
Cat2	453	54.86	5.9
Cat3	366	44.32	9.4
Cat4	333	40.33	11.9

The synthesis of higher alcohols was carried out after the reduction and sulfidation of the catalysts in a fixed bed reactor at 320 °C, 70 bar, and H_2/CO=2. The liquid products were collected at 0 °C and the exit gas was analyzed to measure the CO conversion. The analysis of the liquid products indicates that methanol, ethanol, and propanol were the major products with small amounts of butanol and other higher alcohols. The analysis of exit gas indicated that methane is the major component apart from CO, H_2, and CO_2. Table 6 presents the percentage of CO conversions during 48 hours of continuous synthesis for all the catalysts. Since the percentage of CO conversion can affect the product selectivity, to investigate the effects of particle size on the product selectivity, we changed the GHSV of feed in such a way that for all the catalytic tests the CO conversion was equal. The data in Table 6 confirms this point.

Table 6: The percentage of CO and H_2 conversions for Cat1-Cat4 catalysts

Catalyst	CO Conversion (%)	H_2 Conversion (%)
Cat1	27.70	23.9
Cat2	27.60	24.00
Cat3	27.75	24.2
Cat4	27.70	24.5

Figure 5 presents experimental methanol formation rates versus average molybdenum oxide particle sizes during 48 hours of continuous synthesis. The average molybdenum oxide particle sizes used in this figure are the average of the amounts determined by TEM, XRD, and H_2 chemisorption tests for each catalyst. As shown in this figure, the amount of methanol rises by increasing the average particle size of molybdenum oxide particles. It has been suggested that the sulfidation of the oxides present in the calcined form of the catalysts and the formation of the Mo-K-S species are responsible for the alcohol formation via CO insertion mechanism described above. Furthermore, the theoretical methanol formation rates (g CH_3OH/(hr.gr cat.)) calculated using the described model are shown in Figure 5. This figure confirms that there is very good agreement between the calculated rates and the experimental values. As depicted in Figure 8, methanol synthesis rate rises with increasing the active metal particle size, which indicates that large particles of molybdenum oxide are selective for methanol synthesis.

Figures 6 and 7 show the experimental and theoretical ethanol and higher alcohols (propanol, butanol) formation rates versus average molybdenum oxide particle sizes.

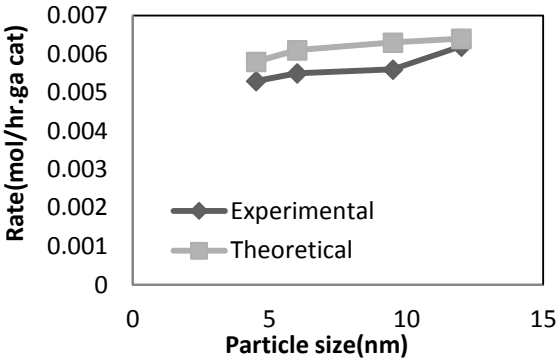

Figure 5: Methanol formation rates for Cat1-Cat4 Catalysts

In contrast to the data shown in Figure 5, ethanol and higher alcohols formation rates are higher for the catalysts with smaller average particle sizes. Smaller particles are selective for ethanol and higher alcohols formation. The decrease in the particle size of the catalytic active sites improves the standard chemical potentials of the components and appreciably affects the adsorption equilibrium. In the case of the catalysts prepared at lower W/S ratios, the drop in Mo particle sizes enhances the adsorption of CO. Ethanol and higher alcohols formation results from the adsorption of carbon monoxide over methanol as a precursor and finally hydrogenation. Increasing the partial pressure of CO on the catalyst surface can suppress the formation of methane via reactions 7 and 12 and will express the reactions 8 and 10,

which in turn increase the ethanol and higher alcohols formation rates. According to the variation in chemical potential during adsorption on catalytic active phase, rate constant changes and in the presence of smaller particles this change is more noticeable. The increase in rate constant during adsorption over active sites makes difference between catalysts that have different particle sizes and thus different rates of reaction can be expected. Comparing the experimental and theoretical formation rates shows that the model successfully predicts the product formation and the distribution of the formation of alcohols within the range of the experiments covered in this study.

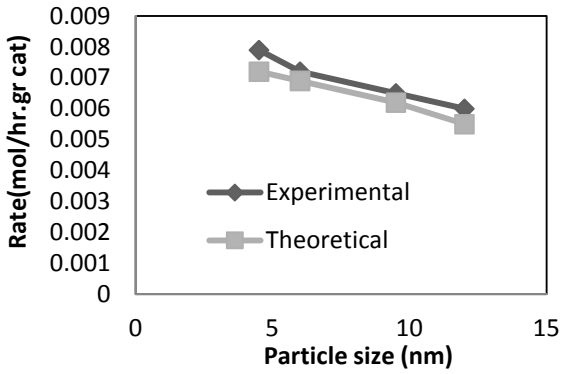

Figure 6: Ethanol formation rates for Cat1-Cat4 Catalysts

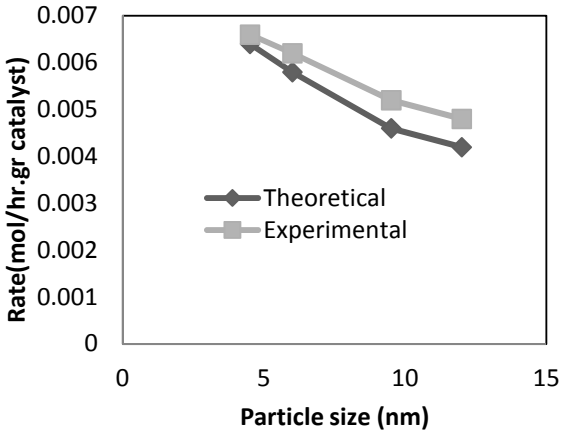

Figure 7: Higher alcohols formation rates for Cat1-Cat4 Catalysts

It should be noted that the theoretical values of rates also depend on kinetic parameters and Polanyi parameters; Polanyi parameter is usually reported to be close to 0.5. Values of kinetic parameters depend on the metal loading and metal-support interactions. Further work is needed to theoretically evaluate the values of η and thus improve the statistical analysis of the results.

CONCLUSIONS

Alkalized MoO_3 nanocatalysts supported on carbon nanotubes were prepared by a microemulsion method and used to produce higher alcohols from synthesis gas. Three different techniques, namely XRD, TEM, and hydrogen chemisorption were used to determine the molybdenum average particle sizes. The preparation of catalysts at low W/S ratios decreased the average MoS_2 particle size from 11.9 to 4.5 nm. Selectivity was found to be dependent on the particle size. The catalysts prepared at a lower water to surfactant ratio, which had lower particle sizes, severely decreased the methanol selectivity but increased ethanol and other higher alcohols selectivity. A model was derived to predict the alcohol formation rates versus catalyst average particle size. The model successfully predicted the product formation and the distribution of the formation of alcohols within the range of the experiments covered in this study. The model can be used for the design and simulation of pilot plants, semi industrial, and commercial plants as well as for the optimization and revamping of existing plants. Further work is needed to theoretically evaluate the values of kinetic parameters and Polanyi parameters and thereby improving the statistical analysis of the results.

REFERENCES

[1] Herman R., "Studies in Surface and Catalyst (Chapter 7)," Amsterdam, Elsevier, **1990**.

[2] Woo H. C. and Park K. Y., "Mixed Alcohol Synthesis from Carbon Monoxide and Hydrogen over Potassium Promoted Molybdenum Carbide Catalysts," *Applied Catalysis*, *75*, **1991**, 267-280.

[3] Jiang M., Bian G. Z., and Fu Y. L., "Effect of the K-Mo Interaction in K-MoS_2/γ-Al_2O_3 Catalysts on the Properties for Alcohol Synthesis from Syngas," *Journal of Catalysis*, *146*, **1994**, 144-154.

[4] Lee J. S., Kim S., Lee K. H., Nam I. S., et al., "Role of Alkali Promoters in K/MoS_2 Catalysts for CO-H_2 Reactions," *Applied Catalysis*, *110*, **1994**, 11-25.

[5] Tatsumi T., Muramatsu A., Yokota K., and Tominga H., "Mechanistic Study on the Alcohol Synthesis over Molybdenum Catalysts: Addition of Probe Molecules to CO-H_2," *Journal of Catalysis*, *115*, **1989**, 388-398.

[6] Surisetty V. R., Tavasoli A., and Dalai A. K., "Synthesis of Higher Alcohols from Syngas over Alkali Promoted MoS_2 Catalysts," *Applied Catalysis*, *365*, **2009**, 243-251.

[7] Iranmahboob J., Toghiani H., and Hill D. O., "Dispersion of Alkali on the Surface of Co-MoS_2/Clay Catalyst: a Comparison of K and Cs as a Promoter for Synthesis of Alcohol," *Applied Catalysis*, *247*, **2003**, 207-218.

[8] Iranmahboob J. and Hill D. O., "Alcohol Synthesis from Syngas over K_2CO_3/CoS/MoS_2 on Activated Carbon," *Catalysis Letters*, *78*, **2002**, 49-56.

[9] Leendert Bezemer G. and Bitter J. H., "Cobalt Particle Size Effects in the Fischer-Tropsch Reaction Studied with Carbon Nanofiber Supported Catalysts," *J. of American Chemical Society*, *128*, **2006**, 39-56.

[10] Parmon V. N., "Thermodynamic Analysis of the Effect of the Nanoparticle Size of the Active Component on the Adsorption Equilibrium and the Rate of Heterogeneous Catalytic Processes," *Physical Chemistry*, *413*, **2007**, 42-48.

[11] Murzin D. Y., "Kinetic Analysis of Cluster Size Dependent Activity and Selectivity," *Journal of Catalysis*, *276*, **2010**, 85-91.

[12] Dmitry Y. M., "Thermodynamic Analysis of Nanoparticle Size Effect on Catalytic Kinetics," *Chemical Engineering Science*, *64*, **2009**, 1046-1052.

[13] Dmitry Y. M., "Size-dependent Heterogeneous Catalytic Kinetics," *Journal of Molecular Catalysis A: Chemical*, *315*, **2010**, 226–230.

[14] Park T. Y., Nam I. S., and Kim Y. G., "Kinetic Analysis of Mixed Alcohol Synthesis from Syngas over K/MoS_2 Catalyst," *Ind. Eng. Chem. Res.*, *36*, **1997**, 5246-5257.

[15] Surisetty V., Dalai A., and Kozinski J., "Intrinsic Reaction Kinetics of Higher Alcohol Synthesis from Synthesis Gas over a Sulfided Alkali-Promoted Co-Rh-Mo Trimetallic Catalyst Supported on Multi-walled Carbon Nanotubes (MWCNTs)," *Energy and Fuels*, *24*, **2010**, 4130–4137.

[16] MartŁnez A. and Prieto G., "Breaking the Dispersion-reducibility Dependence in Oxide-supported Cobalt Nanoparticles," *Journal of Catalysis*, **2007**, *245*, 245-470.

[17] Kim W. Y., Haoka T., Kishida M., and Wakabayashi K., "Hydrogenation of Carbon Monoxide over Zirconia-supported Palladium Catalysts Prepared using Water-in-oil Microemulsion," *Appl. Catal. A*, **1997**, *155,* 283-289.

[18] Tago T., Hanaoka T., Dhupatemiya P., Hayashi H., et al., "Effects of Rh Content on Catalytic Behavior in CO Hydrogenation with Rh-silica Catalysts Prepared using Microemulsion," *Catal. Lett.*, **2000**, *64*(1), 27-31.

[19] Eriksson S., Nylén U., Rojas S., and Boutonnet M., "Preparation of Catalysts from Microemulsions and their Applications in Heterogeneous Catalysis," *Applied Catalysis A: General*, **2004**, *265*, 207–219.

[20] Gunturu A., KuglerE., Cropley J., and Dadyburjor D .,"A Kinetic Model for the Synthesis of High-molecular-weight Alcohols over a Sulfided Co K Mo/C Catalyst," *Ind. Eng. Chem. Res.*, **1998**, *37*, 2107-2115.

Notations

Ads: adsorption term

K_i: equilibrium constants for *i*th reaction

k_i: rate constant for *i*th reaction, kg-cat.mol^{-1}.h^{-1}

P_i: partial pressure of species *i*, MPa

R_i: alkyl group with carbon number *i* (= C_iH_{2i+1})

θ_i: surface coverage of species *i*

s: active site of catalyst

$\mu(r)$: chemical potential

$\mu(\infty)$: chemical potential of a metal particle of an infinite size (bulk like)

α: Polanyi parameter

Appendix

$$r_{iP} = \frac{(\lambda_7 P^{\frac{1}{2}}_{H_2} \theta_{Ri})}{Ads}$$

$$r_{iO} = k_{13}\, \theta_{Ri}$$

$$r_{iE} = \frac{\left[(\frac{\lambda_1}{\lambda_6}) P^{\frac{1}{2}}_{H_2} \theta_{R_i COO} \right]}{A\,ds}$$

$$\lambda_1 = k_6 K_1 [s]_0^2$$

$$\lambda_2 = k_{10} K_2^{\frac{1}{2}} [s]_0^2$$

$$\lambda_3 = k_7 K_2 [s]_0^3$$

$$\lambda_4 = K_5 . K_4 . K_3 . K_1 . K_2^{\frac{3}{2}}$$

$$\lambda_5 = k_{10} [s]_0^2$$

$$\lambda_7 = k_{12} K_2^{\frac{1}{2}} [s]_0^2$$

$$\lambda_8 = k_8 K_1 [s]_0^2$$

$$\lambda_9 = \frac{k_8\ K_1}{k_9 K_2 \left[s\right]_0}$$

$$r_{C_2H_5OH} = \frac{\left[\lambda_2\ P^{\frac{1}{2}}_{H_2} \theta_{R_2O} \right]}{Ads} - \frac{\left[\lambda_5\ P^{\frac{1}{2}}_{C_2H_5OH} \right]}{Ads^2}$$

$$r_{C_3H_7OH} = \frac{\left[\lambda_2\ P^{\frac{1}{2}}_{H_2} \theta_{R_3O} \right]}{Ads} - \frac{\left[\lambda_5\ P^{\frac{1}{2}}_{C_3H_7OH} \right]}{Ads^2}$$

$$r_{C_4H_9OH} = \frac{\left[\lambda_2\ P^{\frac{1}{2}}_{H_2} \theta_{R_4O} \right]}{Ads} - \frac{\left[\lambda_5\ P^{\frac{1}{2}}_{C_4H_9OH} \right]}{Ads^2}$$